ISSN 0022-4766, Journal of Structural Chemistry, 2021, Vol. 62, No. 6, pp. 824-834. © Pleiades Publishing, Ltd., 2021.
Text © The Author(s), 2021, published in Zhurnal Strukturnoi Khimii, 2021, Vol. 62, No. 6, pp. 892-902.

THEORETICAL STUDY OF PENTAVALENT HALOSILICONATES: STRUCTURE AND CHARGE DELOCALIZATION

M. Aichi[1,2], M. Hafied[3]*, and A. Dibi[4]

This study is performed to detect the pentavalent silicon center in the structure of pentavalent-halosiliconate R–O–$Si(CH_3)_3X^-$ and halotrimethylsilyloxyfurane structures (*X*–TMSOF), ($X = F^-$; Cl^-; Br^-) and (R = CH_3–; CH_2–CH_3; –$CH(CH_3)_2$; –CH=CH_2; C_6H_5–). DFT calculations at the B3LYP/6-31G(*d*) level are caried out to understand their structures and charge delocalization. These intermediates are obtained by attacking the silicon center in trimethyl-alkoxysilanes and trimethyl-silyloxyfurane with halogen ions X^-. The results obtained show that the attack by F^- generates more stable structures because of the Si–F bond strong. In the case of Br^- and Cl^-, the structure of intermediates appears as an interaction between the ions and the silicon center. NBO analysis shows that one of F^- lone pairs takes part in the Si–F bond formation. However, the lone pairs of Br^- and Cl^- do not contribute to generate a real bonding.

DOI: 10.1134/S0022476621060020

Keywords: DFT, pentavalent halosiliconates, Si–F bond, NBO, charge delocalization.

INTRODUCTION

Alkoxysilanes are an important kind of organosilicon compounds [1]. Zhang et al. have well studied tetracoordinated silicon compounds and electronic structures of organosilanes in the gas phase and solution [2]. Previously, many studies have been performed on the chemistry of silicon fluorine and chlorine and permitted the investigation of several structures [3, 4].

The hypercoordinated or hypervalent silicon compounds are a class of stable inorganic species such as SiF_6^{2-} [5-7]. It has been of great interest for both experimental [8, 9] and theoretical [10-12] studies. In addition, most organosilicon compounds are generally easy to handle and store for other purposes. They are thermally stable and low toxic [13, 14]. These characteristics make the organosilicon compounds a good choice for diverse organic synthesis methodologies [15, 16] and because of the silicon affinity for electronegative atoms [17, 18]. Desilylation produced via the halogen addition [19] can give halosiliconate intermediate structures (Fig. 1) obtained by introducing fluoride, chloride, and bromide ions into the silicon center of trimethylalkoxysilanes R–O–$Si(CH_3)_3$ and trimethylsilyloxyfurane.

[1]Department of Matter Sciences, Faculty of Sciences and Technology, Abbas Laghrour Khenchela University, Khenchela, Algeria. [2]Department of Chemistry, Faculty of the Exact Sciences and Sciences of the Nature and Life, Mohammed Khidher-Biskra University, Biskra, Algeria. [3]Department of Medicine, Faculty of Medical Sciences, Mustapha Benboulaid Batna 2 University, Batna, Algeria; *hafied_meriem@yahoo.fr. [4]Department of Chemistry, Faculty of Matter Sciences, Batna 1 University, Batna, Algeria. Original article submitted October 7, 2020; revised December 5, 2020; accepted December 12, 2020.

 0022-4766/21/6206-0824 © 2021 by Pleiades Publishing, Ltd.

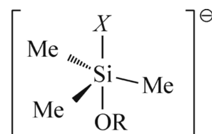

Fig. 1. Structure of halosiliconates (R = Me, Et, ipr, vinyl, aryl, and $X = F^-, Cl^-, Br^-$).

Because of the difficult or even impossible experimental isolation and characterization of these intermediates, this work is based on the theoretical study that allows the investigation of their structures for the following great goals:

– these structures can be used in fundamental studies of hypervalency [20, 21] as well as in numerous theoretical [22, 23] and experimental studies [24, 25].

– the effect of substitutions on pentavalent siliconate are not well known [26].

Furthermore, we mainly focused on the geometry optimization at the B3LYP/6-31G(*d*) level of calculations as a starting point to investigate the most stable structure and estimate many properties of the intermediate systems. The optimized geometries of halosiliconates studied adopt the bipyramidal trigonal shape in the (axial-axial) position for the halogen (*X*) and the alkoxy group (O–R). Moreover, the NBO analysis allowed us to describe the electron density delocalization in *n*- (LP), σ-, and π-donors to explain their ability of Si–*X* formations [27]. Charge delocalization of these intermediates and ^{29}Si chemical shifts can characterize the type of the silicon center.

RESULTS AND DISCUSSION

The following section describes the calculation results for pentavalent halosiliconates $R–O–Si(CH_3)_3X^-$. Halotrimethylsilyloxyfuranes (*X*–TMSOF) are presented in the next secion. All optimized structures are minima on the potential energy surface (number of imaginary frequencies = 0).

Computational chemistry. The calculations were carried out by means of the DFT theory at the B3LYP/6-31G(*d*) level [28]. The geometry of all structures has been fully optimized, and the vibrational frequencies were calculated at the same level to characterize stationary points as minima (number of imaginary frequencies = 0). The charge delocalization was analysed by NBO theory [29]. The ^{29}Si NMR chemical shifts referenced to TMS were calculated by the gauge including atomic orbital (GIAO-DFT/B3LYP/6-31G(*d*)) method [30]. The Gaussian 09 software was used for all calculations [31].

Structure of halosiliconates $R–O–Si(CH_3)_3X^-$. The geometry optimization calculations of halosiliconates provide some results presented in Table 1. Interestingly, we have found that the $R–O–Si(CH_3)_3F^-$ structure is more stable in the case of $R = –CH(CH_3)_2$ where the silicon center adopts fluorine because of its small size, creating a strong Si–F bond. The HOMO–LUMO gaps of the $R–O–Si(CH_3)_3X^-$ halosiliconate structures are listed in Table 1. The $Et–O–Si(CH_3)_3F^-$ structure presents the highest value $\Delta E_{HOMO–LUMO} = 0.57884$ eV. The $R–O–Si(CH_3)_3Cl^-$ structures exhibit approximate values for several groups R. However, for R = -aryl in $R–O–Si(CH_3)_3Br^-$, the structure shows a smaller gap.

In the case of $X = Cl^-$ and $X = Br^-$, the structures reveal a non-bonded interaction between *X* and $R–O–Si(CH_3)_3$; the halogen atom moves away with Si–*X* distances listed in Table 2. Furthermore, Si–O is a nearly double bond; the values are given as 1.70 Å, 1.71 Å, 1.73 Å, and 1.74 Å. The Si–*X* bond shows a convergent value (Table 2). Cl^- and Br^- are labeled with the large negative natural charge values: –0.941 and –0.925 respectively.

NBO analysis. The NBO analysis is a theory for studying hybridization and covalency effects of polyatomic wave functions. It provides the electron density distribution on atoms and bonds and offers the most natural Lewis structure [32, 33]. More precisely, NBOs formed are sets of orthonormal orbitals located at “maximum occupancy”. All settings of these NBOs (polarization coefficients, hybrid atomic compositions, etc.) are mathematically chosen to describe the total density of *n* electrons [34].

TABLE 1. Total Energy, Minimum and Stretching Frequencies, $\Delta E_{HOMO–LUMO}$ Gaps, Dipole Moments and Symmetry of $R–O–Si(CH_3)_3X^-$

$R–O–Si(CH_3)_3X$	R	E, a.u.	$\nu_{streching}$ Si–X bond, cm^{-1}	ν_{min}, cm^{-1}	Dipole, Debye	Symmetry	$\Delta E_{HOMO–LUMO}$, eV
$X = F^-$	Me	–624.317	636.18	83	1.34	C_1	0.28868
	Et	–660.794	640.66	91	3.19	C_1	0.57884
	Aryl	–816.082	723.89	38	1.92	C_1	0.19262
	Vinyl	–662.424	654.72	58	0.73	C_1	0.24410
	Ipr	–702.956	637.65	55	3.53	C_1	0.27396
$X = Cl^-$	Me	–984.708	88.28	56	11.33	C_1	0.21653
	Et	–1024.028	86.08	31	13.32	C_1	0.21315
	Aryl	–1176.452	74.39	52	15.67	C_s	0.25740
	Vinyl	–1022.801	90.55	13	10.75	C_1	0.17751
	Ipr	–1063.345	86.30	18	14.48	C_1	0.20116
$X = Br^-$	Me	–3096.223	78.64	54	8.24	C_1	0.21053
	Et	–3135.543	75.08	23	2.39	C_1	0.20714
	Aryl	–3287.977	88.53	13	8.36	C_s	0.15066
	Vinyl	–3134.316	74.18	46	7.56	C_1	0.17127
	Ipr	–3174.860	76.02	23	11.24	C_1	0.19580

TABLE 2. Natural Charge of Si and X^-, Si–X and Si–O Bonds, Si–O–R Angle

$R–O–Si–(CH_3)_3X$	R	Si–X, Å	Si–O, Å	Si–O–R, deg	X^-	Si
$X = F^-$	Me	1.75	1.85	176.9	–0.718	2.081
	Et	1.83	1.84	109.5	–0.781	2.291
	Aryl	1.67	1.97	52.0	–0.662	2.092
	Vinyl	1.73	1.95	123.9	–0.710	2.071
	Ipr	1.74	1.88	126.0	–0.715	2.084
$X = Cl^-$	Me	3.89	1.71	121.9	–0.941	2.034
	Et	3.88	1.71	122.5	–0.941	2.035
	Aryl	3.67	1.73	146.4	–0.935	2.038
	Vinyl	3.78	1.73	125.4	–0.935	2.034
	Ipr	3.88	1.71	123.6	–0.940	2.036
$X = Br^-$	Me	3.95	1.71	121.9	–0.925	2.032
	Et	2.47	1.71	122.5	–0.924	2.034
	Aryl	4.34	1.70	133.1	–0.903	2.026
	Vinyl	3.84	1.74	124.5	–0.919	2.032
	Ipr	3.94	1.71	123.7	–0.923	2.035

The NBO analysis is a very useful tool for understanding several concepts [35] such as Lewis structures, electron density, bond orders, hybridization, and intermolecular or intramolecular donor–acceptor interactions.

In this study, the NBO analysis gives a very interesting information about the electronic occupancy of the mentioned structures. The fluoride anion in the *isp*–$O–Si(CH_3)_3F^-$ structure indicates four lone pairs with different occupancies LP1 = 1.98580, LP2 = 1.96226, LP3 = 1.95618, LP4 = 1.80945. The low occupation of LP4 reveals that a part of the electron

TABLE 3. ^{29}Si Chemical Shifts δ of R–O–Si– $(CH_3)_3X^-$ Structures Calculated for the TMS Reference $Si(CH_3)_4$

R–O–Si–$(CH_3)_3X$	R	TMS-B3LYP/6-311+G(2*d*,*p*) GIAO, ppm	TMS-HF/6-31G(*d*) GIAO, ppm
$X = F^-$	Me	–152.1	–29.7
	Et	–184.7	–62.3
	Aryl	–142.7	–20.4
	Vinyl	–143.3	–20.9
	Ipr	–184.6	–26.2
$X = Cl^-$	Me	–57.4	+65.0
	Et	–58.2	+64.2
	Aryl	–55.7	+66.7
	Vinyl	–50.8	+71.6
	Ipr	–58.9	+63.5
$X = Br^-$	Me	–56.9	+65.5
	Et	–57.7	+64.8
	Aryl	–62.2	+58.2
	Vinyl	–50.2	+72.2
	Ipr	–58.4	+64.0

density participates in the formation of the Si–F bond. In addition, $CH_3–O–Si(CH_3)_3F^-$ seems to be also labeled with four lone pairs, whereas in $Et–O–Si(CH_3)_3F^-$, we found only three lone pairs. Furthermore, the Si–O distance increases in the following order of substituents: Et (1.84 Å) < CH_3 (1.85 Å) < Ipr (1.87 Å) (Table 3).

As shown in Fig. 2*b*, the geometry optimization indicates that the silicon center is strongly bonded with fluoride (Si–F=1.67 Å). This value is compared with the same bond in free fluorotrimethylsilane $SiF(CH_3)_3$ at the same level of calculations, whereas in the structure *a*, Si–F is 1.73 Å.

These two systems *a* and *b* reveal the loss of O-vinyl and O-aryl groups with Si–O distances being 1.95 Å and 1.97 Å, respectively. The C–O bond is nearly double (1.31 Å in *a* and *b*); the oxygen atom has a negative charge (–0.83 in *a* and –0.81 in *b*).

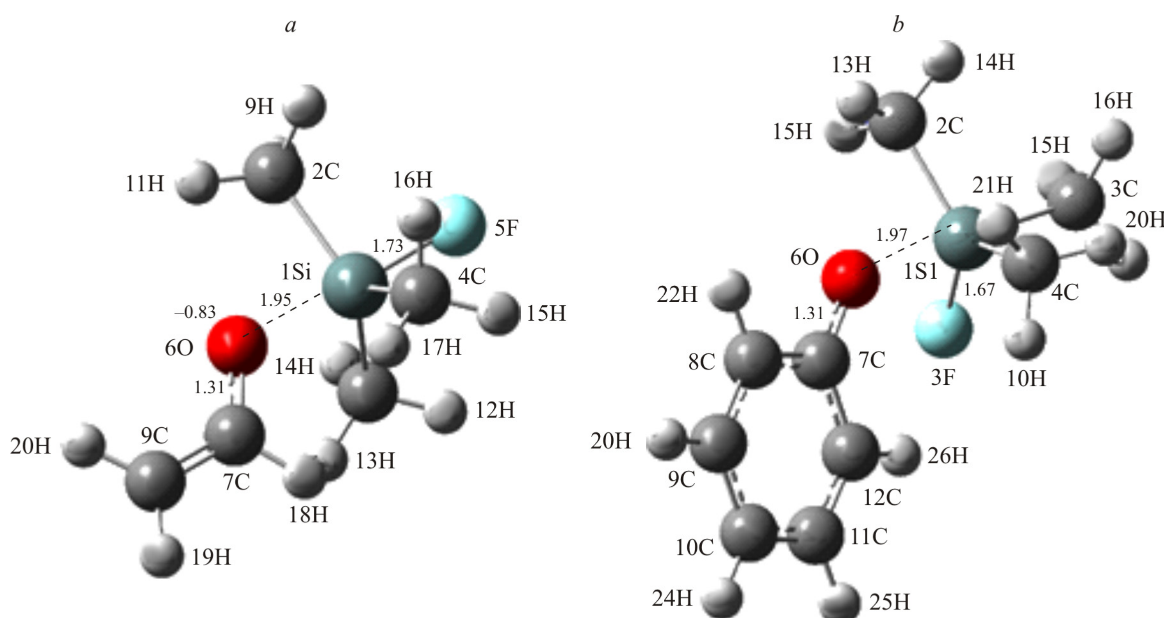

Fig. 2. Non-bonded complexation with the loss of O-vinyl (*a*) and O-aryl groups (*b*).

The NBO analysis permits the calculation of the occupancies of main bonds and lone pairs in these systems. In the structure (*b*), the F^- anion initially has four intact lone pairs. After its introduction into the silicon center, their occupancies are LP1 = 1.98386; LP2 = 1.96416; LP3 = 1.92970; LP4 = 1.78312.

Both LP3 and LP4 participate notably by a charge transfer in the formation of the Si–F bond. Moreover, in the structure (*b*), the oxygen atom received a small electronic charge on behalf of the aryl ring and the Si–O bond to appear in three lone pairs instead of two: LP1 = 1.93970; LP2 = 1.80664; LP3 = 1.73891.

Furthermore, in the structure (*a*), F^- also induces desilylation by the formation of a strong Si–F bond with an occupancy of 1.95081. Therefore, the fluoride anion participates by one of its four lone pairs, and the silicon center loses the O-vinyl group.

^{29}Si NMR chemical shifts of R–O–Si(CH$_3$)$_3$*X*$^-$. The ^{29}Si shifts δ as high as 115 ppm, 226 ppm, and 316 ppm have been observed for R_3Si^+ with R = alkyl, aryl, silyl, respectively [36-39]. However, most examples of silyl cations show an NMR shift in the range 20-100 ppm because of the interaction of the Si center with electron density sources. For classical carbenium ions there is a clear difference between ionic, planar, and covalent tetrahedral species.

It is well understood that ^{29}Si NMR chemical shifts cannot be directly equated to charge densities. Based on this assumption, we have calculated ^{29}Si NMR chemical shifts δ in ppm using the GIAO-HF/6-31G(*d*) method [38] and drawn correlations between the Si–O bond, and NMR ^{29}Si chemical shifts δ of halosiliconate R–O–Si(CH$_3$)$_3$$X^-$ systems.

The ^{29}Si chemical shifts δ (ppm) calculated for R–O–Si–(CH$_3$)$_3$*X* structures and the reference compound tetramethylsilane Si(CH$_3$)$_4$ (TMS) by GIAO-B3LYP/6-311+G(2*d*,*p*) and HF/6-31G(*d*) methods are listed in Table 3.

In this study, fluorosilicate R–O–Si(CH$_3$)$_3$$F^-$ gives ^{29}Si chemical shifts in the range from –62.31 ppm to –20.35 ppm and no linearity was observed in this case. The linearity is established between the Si–O bond and ^{29}Si NMR chemical shifts δ where *X* = Cl^-, Br^- (Fig. 3) and that permits us to get a relationship between these three parameters for the systems. On the other hand, the remaining Si–O bonds present a nearly linear correlation with ^{29}Si NMR chemical shifts δ in the case of Me, Et, and ipr substituents.

We studied halotrimethylsilyloxyfurane *X*–TMSOF structures (Fig. 4) where we have only changed X^- and kept the alkoxyfurane group. The DFT calculations at the B3LYP/6-31G(*d*) level give some information about their structures and electron density charges.

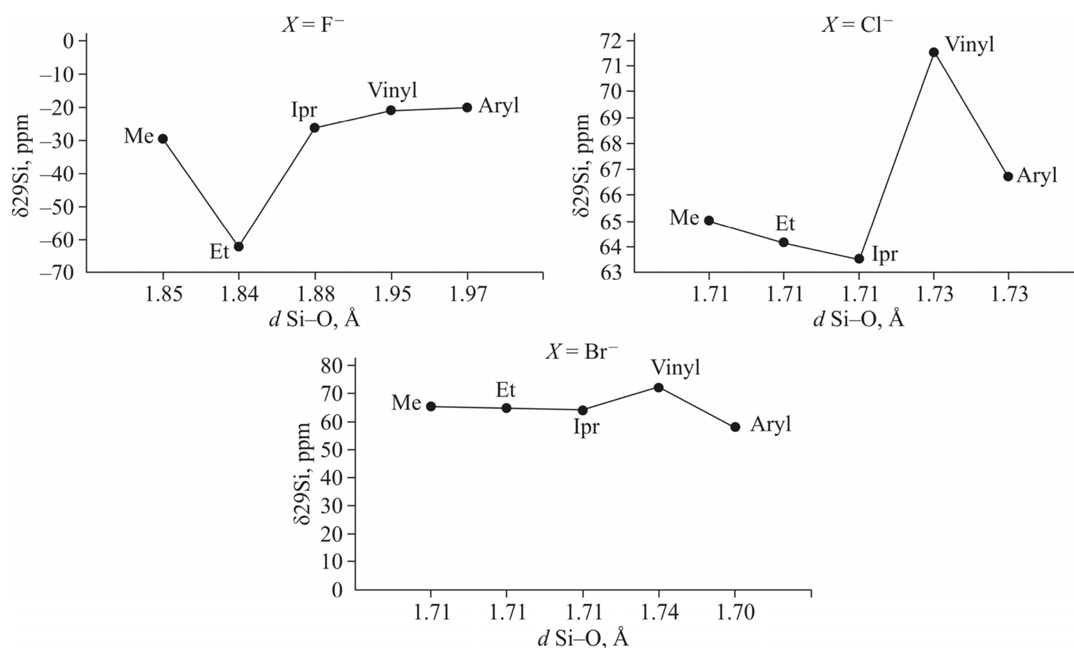

Fig. 3. Correlation between the Si–O length (Å) and ^{29}Si NMR δ (ppm) of R–O–Si(CH$_3$)$_3$*X* (*X* = F, Cl, Br) calculated by the GIAO-HF/6-31G(*d*) method.

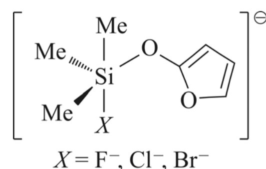

Fig. 4. Halotrimethylsilyloxyfurane X–TMSOF ($X = F^-, Cl^-, Br^-$).

***X*–TMSOF structure.** After introducing *X*, the geometry optimization allows us to explore that in the case of fluoride–TMSOF. The Si–O distance appears as a weak bond with a length of 1.85 Å. However, Si–F seems to be a strong bond of 1.73 Å.

This structure prefigures the formation of the tetra-coordinated silicon center $(CH_3)_3SiF$ and a loss of the oxyfurane group. In the case of $X = Cl^-$ or Br^-, the Si–O bond is 1.73 Å, however Si–*X* are valued to be 4.25 Å and 4.29 Å, respectively.

In Table 4, the minimum frequency (ν_{min}) indicates that all the *X*–TMSOF structures are the minima. Moreover, $\Delta E_{HOMO–LUMO}$ gaps show that in the case of the F–TMSOF structure (ΔE), the gap has a greater value compared with those of Cl–TMSOF and Br–TMSOF, which reflects the stabilization of the HOMO due to the electronegativity of the fluorine atom. The stretching frequency of Si–*X* bonds reveals that the Si–F bond is stronger than the Si–Cl one, which is confirmed by the Si–F of 1.71 Å (Table 4). The Si–Br bond is abnormally long (4.29 Å) and is the weakest bond. The reaction between a nucleophile *X* (F–, Cl–) and the substrate SiH4 has been studied in [40]. The optimal lengths of silicon chlorine and silicon fluorine bonds are 2.1 Å and 1.6 Å, respectively.

F–TMSOF shows a long Si–O bond (1.85 Å) which estimates a loss of the fragment $Si(CH_3)_3F^-$. However, in the case of $Cl–TMSOF^-$ and $Br–TMSOF^-$, this bond is equal to 1.71 Å. Besides, the NBO charge clearly shows that the silicon center bears positive net charge (+2.1 for F–TMSOF and +2.02 for Cl–TMSOF and Br–TMSOF). F^-, Cl^- and Br^- are labeled with a negative charge (–0.70, –0.93, and –0.90, respectively).

Table 5 shows that the fluoride lone pair LP4 in F–TMSOF contributes to produce the Si–F bond with a 1.921 occupancy and the Si 7.95%, F 92.05% percentage structure. However, chloride and bromide keep well their four lone pairs, thereafter only a very weak contribution is noted.

The HOMO shows that the lone pair orbital is mainly located on chloride in Cl–TMSOF, weakly located on the fluoride atom in F–TMSOF and does not appear on bromide in Br–TMSOF.

The LUMO of Cl–TMSOF is localized on the oxyfuran skeleton and is similar to the LUMOs of F–TMSOF and Br–TMSOF (Fig. 5). There is much more electron density in the vicinity of the silicon atom for all the studied molecules.

TABLE 4. Total Energies, the Lowest Frequencies, $\Delta E_{HOMO–LUMO}$ Gaps, Dipole Moments and Symmetry of *X*–TMSOF

X–TMSOF	*E*, a.u.	$\nu_{streching}$ Si–*X* bond, cm^{-1}	ν_{min}, cm^{-1}	Dipole, Debye	Symmetry	$\Delta E_{HOMO–LUMO}$, eV
X = F	–813.85	708.43	28.25	2.87	C1	0.2124
X = Cl	–1174.24	105.33	27.7	10.26	C1	0.1886
X = Br	–3285.75	97.47	15.98	7.85	C1	0.1805

TABLE 5. Lone Pair Occupancies of Halogen, Si–*X* and Si–O Bonds, Si–O–C Angle, Natural Charges of Si and *X* in *X*–TMSOF Structures

X–TMSOF	Si–*X* bond, Å	Si–O bond, Å	Si–O–C, deg	Si	X^-	LP1	LP2	LP3	LP4
X = F	1.71	1.85	128.7	+2.10	–0.70	1.984	1.956	1.955	–
X = Cl	4.25	1.71	128.9	+2.02	–0.93	1.999	1.985	1.983	1.954
X = Br	4.29	1.71	130.7	+2.02	–0.90	1.999	1.980	1.979	1.945

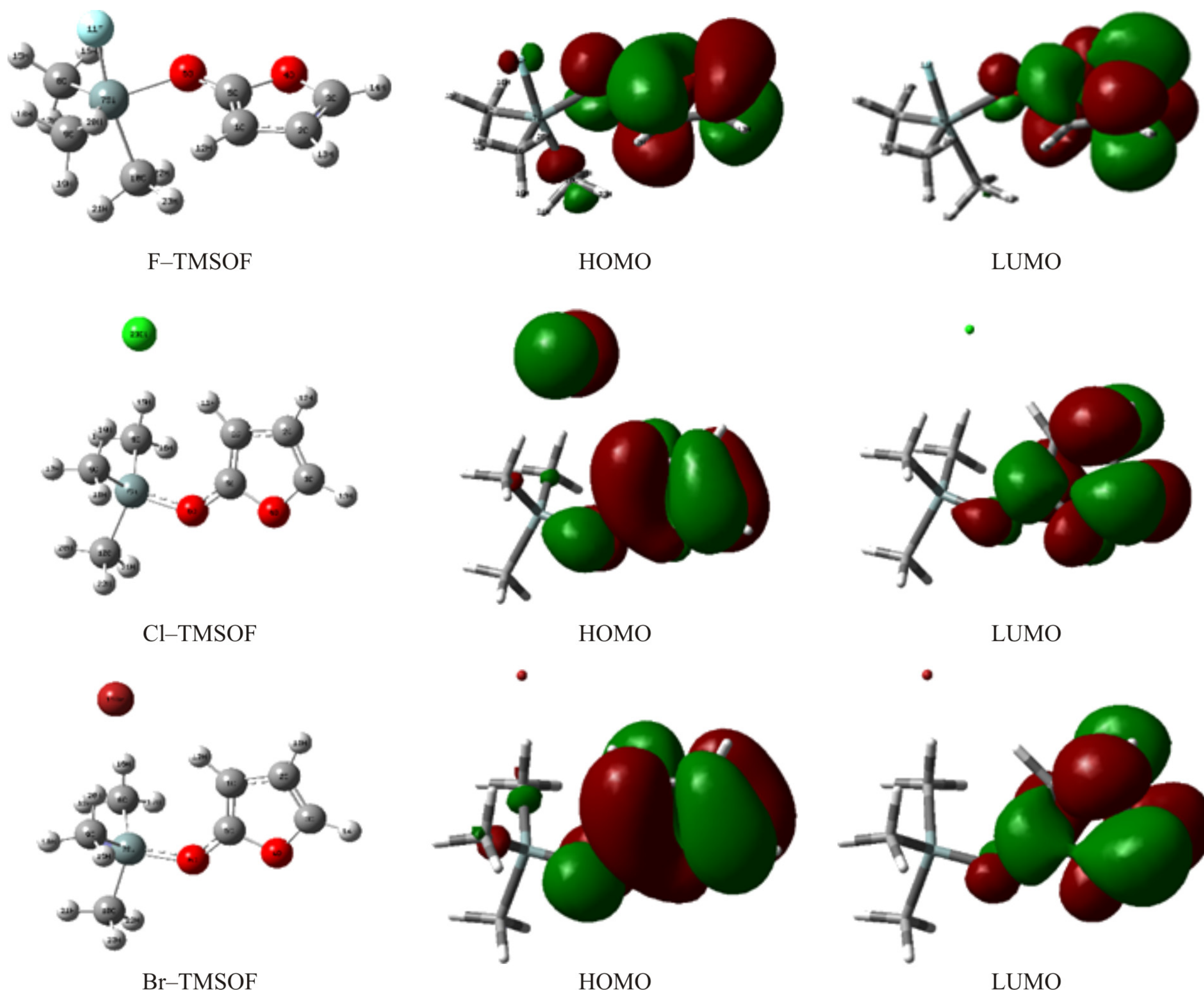

Fig. 5. HOMOs and LUMOs of *X*–TMSOF structures.

Charge delocalization in *X*–TMSOF structures. The NBO analysis is used to examine all possible interactions between Lewis-type occupied (donor) NBOs and non-Lewis-type vacant (acceptor) orbitals. The interactions are determined by the second order perturbation approach [41]. This approach is used to calculate the stabilization energies of orbital interactions between the donor and acceptor NBOs. The stabilization energy $\Delta Ei \rightarrow j$ is the energy difference between the donor and acceptor orbitals.

For each NBO donor (i) and NBO acceptor (j), the stabilization energy $E(2)$ associated with the electron delocalization $i \rightarrow j$ is given by the following expression:

$$E^{(2)} = q_i \frac{(F_{i,j})^2}{\varepsilon_j - \varepsilon_i},$$

where q_i is the occupation of the i donor orbital, ε_i and ε_j are the energies of the orbitals (i.e. the diagonal elements of the Fock matrix), F_{ij} is the non-diagonal Fock element. Table 6 lists the calculated NBO occupancies.

In F–TMSOF, it is important to mention that the σ(Si–F) bond contained 92.05% of fluorine and 7.95% of silicon and was formed from the $sp^{1.26}$ hybrid on fluorine (which is a mixture of 44.13% *s*, 55.75% *p*, and 0.13% *d*). The σ(Si–O6) bond is produced from the $sp^{2.38}$ hybrid on oxygen (which is a mixture of 29.58% *s*, 70.37% *p*, and 0.05% *d*). Cl–TMSOF indicates that the σ(Si–O6) bond is formed from the $sp^{1.78}$ hybrid on oxygen (which is a mixture of 35.93% *s*, 64.00% *p*, and 0.08% *d*). The σ(Si–C10) bond is produced from the $sp^{2.28}$ hybrid on carbon (which is a mixture of 30.44% *s*, 69.54% *p*, and 0.03% *d*). In the Br–TMSOF structure, the σ(C1–C2) bond is obtained from the $sp^{1.75}$ hybrid on C1 (which is a mixture

TABLE 6. Bond Distances, Occupancies, and Percentage of Hybrid Atomic Orbitals of *X*–TMSOF

Structure	Aims bond	Distance, Å	Occupancy	% of atoms in bond	Hybrid	AO,%
F–TMSOF	C1–C2	1.44	1.967	49.35C150.65C2	$sp^{2.03}$	s(32.96) p(67.00) d(0.04)
	C2–C3	1.36	1.987	50.95C249.05C3	$sp^{1.90}$	s(34.41) p(65.54) d(0.04)
	C1–C5	1.38	1.985	50.72C149.28C5	$sp^{2.03}$	s(32.96) p(66.99) d(0.05)
	Si–C8	1.93	1.942	21.52Si78.48C8	$sp^{2.15}$	s(31.78) p(68.20) d(0.02)
	Si–C9	1.94	1.924	21.42Si78.58C9	$sp^{2.17}$	s(31.53) p(68.45) d(0.02)
	Si–C10	1.98	1.893	17.53Si82.47C10	$sp^{1.14}$	s(31.87) p(68.12) d(0.01)
	Si–F	1.71	1.946	7.95Si92.05F	$sp^{1,26}$	s(44.13) p(55.75) d(0.13)
	Si–O6	1.85	1.921	9.09Si90.91O6	$sp^{2.38}$	s(29.58) p(70.37) d(0.05)
	LP3F	–	1.954	–	$sp^{47.86}$	s(2.05) p(97.90) d(0.06)
	LP1O6	–	1.917	–	$sp^{2.03}$	s(33.03) p(66.91) d(0.06)
	σ*C1–C2	–	0.010	50.65C149.35C2	$sp^{2.03}$	s(32.96) p(67.00) d(0.04)
	π*C2–C3	–	0.014	49.05C250.95C3	$sp^{1.90}$	s(34.41) p(65.54) d(0.04)
	σ*Si–O6	–	0.108	90.91Si9.09O6	$sp^{2.38}$	s(29.58) p(70.37) d(0.05)
Cl–TMSOF	Si–C8	1.88	1.969	26.32 Si73.68C	$sp^{2.53}$	s(28.30) p(71.66) d(0.04)
	Si–C9	1.86	1.969	26.32Si73.68C	$sp^{2.53}$	s(28.30) p(71.67) d(0.04)
	Si–C10	1.89	1.973	24.43Si75.57C	$sp^{2.28}$	s(30.44) p(69.54) d(0.03)
	Si–Cl	4.25	–	–	–	–
	Si–O6	1.71	1.968	12.85Si87.15O6	$sp^{1.78}$	s(35.93) p(64.00) d(0.08)
	LP4Cl	–	1.953	–	$sp^{7.78}$	s(11.39) p(88.61) d(0.00)
	LP1O6	–	1.928	–	$sp^{2.52}$	s(28.36) p(71.57) d(0.07)
	σ*C1–C2	–	0.010	50.66C149.34C2	$sp^{2.15}$	s(31.69) p(68.26) d(0.05)
	π*C2–C3	–	0.013	49.47C250.53C3	$sp^{1.93}$	s(34.17) p(65.78) d(0.05)
	σ*Si–O6	–	0.065	87.15Si12.85O6	$sp^{3.82}$	s(20.20) p(77.12) d(2.69)
Br–TMSOF	σC1–C2	1.44	1.962	49.34C150.66C2	$sp^{2.15}$	s(31.72) p(68.24) d(0.05)
	πC2–C3	1.36	1.988	50.55C249.45C3	$sp^{1.92}$	s(34.19) p(65.77) d(0.05)
	C1–C5	1.37	1.985	49.96C150.04C5	$sp^{2.11}$	s(32.12) p(67.83) d(0.06)
	Si–C8	1.88	1.969	26.36Si73.64C8	$sp^{2.58}$	s(27.56) p(71.11) d(1.33)
	Si–C9	1.88	1.969	26.36Si73.64C9	$sp^{2.58}$	s(27.56) p(71.11) d(1.33)
	Si–C10	1.89	1.973	24.42Si75.58C10	$sp^{2.98}$	s(24.77) p(73.90) d(1.33)
	Si–Br	4.29	–	–	–	–
	σSi–O6	1.71	1.968	12.879Si87.21O	$sp^{1.75}$	s(36.29) p(63.63) d(0.07)
	LP4Br	–	1.945	–	$sp^{7.62}$	s(11.60) p(88.40) d(0.00)
	LP1O6	–	1.926	–	$sp^{2.62}$	s(27.64) p(72.29) d(0.07)
	σ*C1–C2	–	0.010	50.66C149.34C2	$sp^{2.15}$	s(31.72) p(68.24) d(0.05)
	π*C2–C3	–	0.013	49.45C150.55C3	$sp^{1.92}$	s(34.19) p(65.77) d(0.05)
	σ*Si–O6	–	0.065	87.21Si12.79O6	$sp^{1.75}$	s(36.29) p(63.63) d(0.07)

of 31.72% *s*, 68.24% *p*, and 0.05% *d* atomic orbitals). In addition, σ(Si–C8) and σ(Si–C9) bonds are produced from the $sp^{2.58}$ hybrid on C8 and C9 respectively (which are a mixture of 27.56% *s*, 71.11% *p*, and 1.33% *d*). The σ(Si–O6) bond is obtained from the $sp^{1.75}$ hybrid on oxygen (which is a mixture of 36.29% *s*, 63.63% *p*, and 0.07% *d*).

The electron density delocalization between occupied Lewis type (bond or lone pair) NBOs and formally unoccupied (antibonding or Rydberg) non-Lewis NBOs corresponds to a stable donor–acceptor interaction. The perturbation energies of donor–acceptor interactions are presented in Table 7.

The most significant interactions in F–TMSOF corresponding to the interaction of the furan ring are given as LP2O6 → π*(C1–C5) with 52.83 kcal/mol, LP2O4 → π*(C1–C5) with 29.80 kcal/mol, and π(C1–C5) → π*(C2–C3) with

TABLE 7. Second Order Perturbation Theory Analysis of the Fock Matrix in the NBO Basis of *X*–TMSOF Structures

Structure	Donor (*i*)	Type	Acceptor (*j*)	Type	$E^{*(2)\#1}$, Kcal/mol	$E(j)–E(i)^{\#2}$, a.u.	$F(i,j)^{\#3}$, a.u.
F–TMSOF	Si–C8	σ	Si–O6	σ*	4.55	0.84	0.056
			Si–C10	σ*	2.85	0.97	0.131
			Si–F	σ*	29.02	1.02	0.155
	Si–C9	σ	Si–C10	σ*	19.89	0.97	0.125
			Si–F	σ*	24.92	1.02	0.144
	Si–C10	σ	Si–O6	σ*	47.17	0.76	0.169
			Si–C8	σ*	21.74	0.69	0.111
			Si–C9	σ*	19.85	0.67	0.104
			Si–F	σ*	30.76	0.95	0.152
	Si–F	σ	Si–O6	σ*	27.57	1.26	0.169
			Si–C10	σ*	19.39	1.39	0.148
			Si–C8	σ*	13.51	1.19	0.113
			Si–C9	σ*	12.26	1.17	0.107
	C1–C2	σ	C5–O6	σ*	8.25	1.14	0.087
	C1–C5	π	C2–C3	π*	21.17	0.28	0.071
	C2–C3	π	C1–C5	π*	9.32	0.31	0.052
	F	LP1	Si–C10	σ*	6.96	1.35	0.088
	O4	LP2	C1–C5	π*	29.80	0.35	0.094
	O6	LP2	C1–C5	π*	52.83	0.30	0.118
Cl–TMSOF	C1–C2	σ	C5–O6	σ*	10.23	1.04	0.092
	C1–C5	π	C2–C3	π*	18.06	0.29	0.067
	O4	LP2	C1–C5	π*	28.58	0.37	0.092
			C2–C3	π*	24.70	0.36	0.084
	O6	LP1	C1–C5	π*	9.29	1.09	0.091
		LP2	C1–C5	π*	32.49	0.36	0.101
	Cl	LP4	C1–H12	σ*	6.00	0.75	0.060
			C8–H15	σ*	2.44	0.70	0.037
			C9–H19	σ*	2.46	0.70	0.037
Br–TMSOF	C1–C2	σ	C5–O6	σ*	10.21	1.04	0.092
	C1–C5	π	C2–C3	π*	18.10	0.29	0.067
	O4	LP2	C1–C5	π*	28.59	0.37	0.092
			C2–C3	π*	24.82	0.36	0.084
	O6	LP1	C1–C5	π*	9.44	1.08	0.091
			O4–C5	σ*	5.99	0.84	0.064
		LP2	C1–C5	π*	32.87	0.36	0.101
	Br	LP4	C1–H12	σ*	5.24	0.74	0.056
			C8–H16	σ*	3.69	0.70	0.046
			C9–H20	σ*	3.69	0.70	0.046

[*] Only interactions with the highest energy (strongest stabilization) are listed.
[#1] E^2 means the hyperconjugative interaction energy (stabilization energy).
[#2] Energy difference between *i* donor and and *j* acceptor NBOs.
[#3] $F(i,j)$ is the Fock matrix element between *i* and *j* NBOs.

21.17 kcal/mol. Around the silicon center σ(Si–C10) → σ*(Si–O6) with 47.17 kcal/mol and σ(Si–C8) → σ*(Si–F) with 29.02 kcal/mol, σ(Si–C9) → σ*(Si–F) with 24.92 kcal/mol, and σ(Si–F) → σ*(Si–O6) with 27.57 kcal/mol. Hence, these findings give stronger stabilization of the structure.

The important interactions observed in Cl–TMSOF are illustrated as π(C1–C5) → π*(C2–C3) with 18.06 kcal/mol, LP2O4 → π*(C1–C5) with 28.58 kcal/mol, and LP2O6 → π*(C1–C5) with 32.49 kcal/mol. Br–TMSOF is also characterized by the interaction π(C1–C5) → π*(C2–C3) of 18.10 kcal/mol, LP2O4 → π*(C1–C5) of 28.59 kcal/mol, and LP2O6 → π*(C1–C5) of 32.87 kcal/mol.

CONCLUSIONS

The interaction of fluoride, chloride, and bromide anions with the silicon center of trimethylalkoxysilane gives the penta-coordinated silicon atom only in the case of fluoride. The introduction of fluoride into the silicon center allows the formation of the strong Si–F bond and predicts the loss of the O-R group in all the studied structures (Si–O is at least 1.85 Å). In addition, both structures with chloride and bromide are characterized by non-bonded interactions that appear between the silicon center and added *X*.

In V–OFTMS and A–OFTMS structures, the non-bonded interaction between the oxygen and silicon atoms seems to be a strong electrostatic attraction that leads to an extraordinary non-bonded interaction.

The existence of the oxyfurane group in all *X*–TMSOF structures induces a high electron density in the vicinity of the silicon center. Furthermore, in HOMOs, the highest electron density appears on the lone pair of the chloride ion. The NBO analysis has provided the detailed insight into the type of hybridization and the nature of bonding in *X*–TMSOF structures. The maximum occupancy values for most interacting NBOs of *X*–TMSOF structures are mainly controlled by the *p* character of the hybrid orbitals.

ACKNOWLEDGMENTS

The authors are grateful to Bahouaddine Tangour, Professor at El-Manar-Tunis University for supporting this research by the Gaussian 09 program and for the helpful comments that we greatly appreciate.

CONFLICT OF INTERESTS

The authors declare that they have no conflict of interests.

REFERENCES

1. M. A. Pigaliva, V. Elmanovich, M. Timnikov, and A. M. Muzafarov. *Polym. Sci*., *Ser. B*, **2016**, *58*, 270.
2. C. Zhang, P. Patschinski, S. D. Stephenson, R. Panisch, J. H. Wender, M. C. Holthausen, and H. Zipse. *Phys. Chem. Chem. Phys*., **2014**, *16*, 16650.
3. I. Mohamed and K. Subramani. *E-J. Chem*., **2008**, *5*, 136–143.
4. S. S. Sen and W. H. Roesky. *Chem. Commun*., **2018**, *54*, 5057.
5. V. V. Negrebetsky, S. N. Tandura, and Yu. I. Baukov. *Russ. Chem. Rev*., **2009**, *78*, 51.
6. S. R. Ghadwal, P. Kevin, D. Birger, G. P. Jones, and W. H. Roesky. *Inorg. Chem*., **2011**, *50*, 364.
7. F. Bitto, K. Kraushaar, U. Böhme, E. Brendler, and J. Wagler. *Eur. J. Inorg. Chem*., **2013**, *35*, 2962.
8. D. K. Onan, T. A. McPhail, H. C. Yoder, and W. R. Hillyard. *J. Chem. Soc*., *Chem. Commun*., **1978**, *5*, 210.
9. A. R. Bassindale, P. G. Taylor. In: The Chemistry of Organic Silicon Compounds / Eds. S. Patai, Z. Rappoport. John Wiley & Sons: Chichester, UK, **1989**, Part 1, 839–892.
10. C. Marsden. *J. Inorg. Chem*., **1983**, *22*, 3178.

11. N. Kocher, J. Henn, B. Gostevskii, D. Kost, and I. Kalikhman. *J. Am. Chem. Soc*., **2004**, *126*, 5568.
12. C. W. So, H. W. Roesky, J. Magull, and R. B. Oswald. *Angew. Chem*., *Int. Ed. Engl*., **2006**, *45*(24), 3948.
13. C. A. Burkhard, E. G. Rochow, and H. S. Booth, J. Hartt. *Chem. Rev*., **1947**, *41*,149**.**
14. H. Gilman and G. E. Dunn. *Chem. Rev*., **1953**, *52*, 115.
15. W. P. Weber. Silicon Reagents for Organic Synthesis. Springer-Verlag: New York, **1983**.
16. I. Fleming, A. Barbero, and D. Walter. *Chem. Rev*., **1997**, *97*, 2192.
17. C. Chuit, R. J. Corriu, C. Reye, and J. C. Young. *Chem. Rev*., **1993**, *93*, 1448.
18. D. Kost and I. Kalikhman. Hypervalent Silicon Compounds. In: The Chemistry of Organic Silicon Compounds / Eds. Z. Rappoport, Z. Rappoport and Y. Apeloig. Wiley: Chichester, **1998**.
19. I. H. Krouse and P. G. Wenthold. *J. Am. Soc. Mass Spectrom*., **2005**, *16*, 697–707.
20. D. J. Hjdasz and R. R. Squires. *J. Am. Chem. Soc*., **1986**, *108*, 3139–3140.
21. R. R. Holmes. *Chem. Rev*., **1990**, *90*, 17–31.
22. M. S. Gordon, L. P. Davis, L. W. Burggraf, and R. Damrauer. *J. Am. Chem. Soc*., **1986**, *108*, 7889–7893.
23. J. A. Deiters and R. R. Holmes. *J. Am. Chem. Soc*., **1987**, *109*, 1686–1692.
24. M. L. P. da Silva and J. M. Reveros. *J. Mass Spectrom*., **1995**, *30*, 733–740.
25. J. C. Sheldon, R. N. Hayes, and J. H. Bowie. *J. Am. Chem. Soc*., **1984**, *106*, 7711–7715.
26. T. Veszpremi, Y. Harada, K. Ohno, and H. J. Mutoh. *J. Organomet. Chem*., **1984**, *266*, 9–16.
27. N. Lühmann, R. Panisch, and T. Müller. *Appl. Organomet. Chem*., **2010**, *24*, 537.
28. T. Ziegler. *Chem. Rev*., **1991**, *91*, 667.
29. X. Shu-Hong and Z. Ming-yu. *Chem. Phys. Lett*., **2006**, *421*, 447.
30. K. Wolinski, J. F. Hinton, and P. Pulay. *J. Am. Chem. Soc*., **1990**, *112*, 8260.
31. M. J. Frisch, G. W. Trucks, H. B. Schlegel, G. E. Scuseria, M. A. Robb, J. R. Cheeseman, G. Scalmani, V. Barone, B. Mennucci, G. A. Petersson, H. Nakatsuji, M. Caricato, X. Li, H. P. Hratchian, A. F. Izmaylov, J. Bloino, G. Zheng, J. L. Sonnenberg, M. Hada, M. Ehara, K. Toyota, R. Fukuda, J. Hasegawa, M. Ishida, T. Nakajima, Y. Honda, O. Kitao, H. Nakai, T. Vreven, J. A. Montgomery Jr., J. E. Peralta, F. Ogliaro, M. Bearpark, J. J. Heyd, E. Brothers, K. N. Kudin, V. N. Staroverov, R. Kobayashi, J. Normand, K. Raghavachari, A. Rendell, J. C. Burant, S. S. Iyengar, J. Tomasi, M. Cossi, N. Rega, J. M. Millam, M. Klene, J. E. Knox, J. B. Cross, V. Bakken, C. Adamo, J. Jaramillo, R. Gomperts, R. E. Stratmann, O. Yazyev, A. J. Austin, R. Cammi, C. Pomelli, J. W. Ochterski, R. L. Martin, K. Morokuma, V. G. Zakrzewski, G. A. Voth, P. Salvador, J. J. Dannenberg, S. Dapprich, A. D. Daniels, Ö. Farkas, J. B. Foresman, J. V. Ortiz, J. Cioslowski, and D. J. Fox. Gaussian 09. Gaussian, Inc.: Wallingford, CT, **2009**.
32. A. E. Reed, R. B. Weinstock, and F. Weinhold. *J. Chem. Phys*., **1985**, *83*, 746.
33. Valency and Bonding: A Natural Bond Orbital Donor-Acceptor Perspective / Eds. F. Weinhold and C. R. Landis. Cambridge University Press, **2005.**
34. E. D. Glendening, C. R. Landis, and F. Weinhold. *J. Comput. Chem*., **2013**, *34*, 1437.
35. F. Weinhold. Natural Bond Orbital Methods. In: Encyclopedia of Computational Chemistry / Eds. P. von Ragué Schleyer, N. L. Allinger, T. Clark, J. Gasteiger, P. A. Kollman, H. F. Schaefer, and P. R. Schreiner. Wiley, **2002**.
36. G. L. Larson. Recent Synthetic Applications of Organosilanes. In: Organic Silicon Compounds / S. Patai, and Z. Rappoport. Wiley: Chichester, UK, **1989.**
37. A. Sekiguchi, R. Kinjo, and M. Ichinohe. *Science*, **2004**, *305*, 1757.
38. H. Ottosson and A. M. Eklöf. *Coord. Chem. Rev*., **2007**, *252*, 1314.
39. E. C. Lee, D. Kim, P. Jurecka, P. Tarakeshwar, and P. Hobza. *J. Phys. Chem. A*, **2007**, *111*, 3457.
40. M. El Idrissi, A. Zeroual, and A. El Hajbi. *Int. J. Innovation Appl. Stud*., **2014**, *5*, 260.
41. Essentials of Computational Chemistry, 2nd ed. / Ed. C. J. Cramer. John Wiley & Sons, **2004**.